



POLITECNICO
MILANO 1863



Politecnico di Milano

Spacecraft Attitude Dynamics

Project group: 68

Project number: 360



Team members

| Person Code | Surname | Name | Bachelor | University |
|-------------|----------|----------|--|-------------------------------------|
| 10663873 | Degener | Martín | BS. Aeronautical and Astronautical Engineering | Purdue University |
| 10647645 | Ashfaq | Haseeb | BS. Aerospace Engineering | Politecnico di Milano |
| 10882032 | Aranda | Fernando | BS. Aerospace Engineering | Universitat Politècnica de València |
| 10913819 | Albiñana | Carlos | BS. Aerospace Engineering | Universitat Politècnica de València |

Project Specifications

| | Assigned Specification | Modifications | Motivation for Modification |
|---------------------|------------------------------------|----------------------|-------------------------------------|
| Platform | 12U CubeSat | - | - |
| Attitude Parameters | Quaternions | - | - |
| Mandatory Sensors | 3 axis Magnetometer | Added Horizon Sensor | Required for Attitude Determination |
| Actuators | 3 Magnetorquers 1 Inertia Wheel | - | - |

Contents

| | |
|---|-----------|
| Introduction | 1 |
| 1 Mission Description and Requirements | 2 |
| 1.1 Mission Phases | 3 |
| 1.2 Spacecraft Geometry | 3 |
| 2 Dynamics and Kinematics modelling | 4 |
| 2.1 Dynamics | 4 |
| 2.2 Kinematics | 4 |
| 3 Environment modelling | 5 |
| 3.1 Environment modelling | 5 |
| 3.1.1 Orbit Propagation | 5 |
| 3.1.2 Aerodynamic Drag | 5 |
| 3.1.3 Magnetic Field and Disturbance | 6 |
| 3.1.4 Gravity Gradient | 7 |
| 4 Sensor modelling | 8 |
| 4.1 Sensors | 8 |
| 4.1.1 Magnetometer - HMC5983 | 8 |
| 4.1.2 Earth Horizon Sensor - CubeSense Earth Gen 2 | 8 |
| 4.2 Sensor modelling | 8 |
| 4.2.1 Magnetometer | 9 |
| 4.2.2 Earth Horizon Sensor | 9 |
| 4.3 Attitude Determination - Algebraic Method | 10 |
| 5 Control Logic | 11 |
| 5.1 Detumbling - B-Dot Method | 11 |
| 5.2 Slew Manoeuvre and Nadir Pointing - LQR and LQE logic | 11 |
| 5.2.1 State-Space Representation | 12 |
| 5.2.2 Control Design | 13 |
| 6 Actuator modelling | 14 |
| 6.1 Actuator Modelling | 14 |
| 6.1.1 Detumbling | 15 |
| 6.1.2 Slew and Pointing | 15 |
| 7 Simulation | 16 |
| 7.1 Angular Rates | 16 |
| 7.2 Pointing performance | 17 |
| Conclusion | 19 |

List of Figures

| | | |
|-----|---|----|
| 1.2 | Spacecraft Geometry | 3 |
| 3.1 | Air Drag Validation | 6 |
| 3.2 | Magnetic Field Validation | 7 |
| 3.3 | Gravity Gradient Validation | 7 |
| 4.1 | Magnetometer - HMC5983 | 8 |
| 4.2 | Earth Horizon - CubeSense | 8 |
| 6.1 | Magnetorquer - CR0020 | 14 |
| 6.2 | Inertial Wheel - CubeWheel L | 14 |
| 7.1 | Simulink Model | 16 |
| 7.2 | Time evolution of angular velocities | 17 |
| 7.3 | Pointing Error Distribution | 17 |
| 7.4 | SC pointing performance - No Control vs Control | 18 |
| 7.5 | Time Evolution of quaternions - Control enabled | 18 |

List of Tables

| | | |
|-----|---|---|
| 1.1 | Orbital Parameters of the Mission | 2 |
| 3.1 | Disturbance torques | 5 |
| 3.2 | Density Model | 6 |

Nomenclature

Air Drag

| Symbol | Description | Code | Value |
|--------|------------------|------|-------|
| C_D | Drag coefficient | CD | 2.2 |

Geometry of Spacecraft

| Symbol | Description | Code | Value |
|--------------------|--|-------------|---|
| I_x | Inertia in X axis | Ix | 0.6324 kg m^{-2} |
| I_y | Inertia in Y axis | Iy | 0.4084 kg m^{-2} |
| I_z | Inertia in Z axis | Iz | 0.4491 kg m^{-2} |
| J | Inertia matrix | J | $\begin{pmatrix} I_x & 0 & 0 \\ 0 & I_y & 0 \\ 0 & 0 & I_z \end{pmatrix} \text{ kg m}^{-2}$ |
| J^{-1} | Inverse inertia matrix | invJ | $J^{-1} \text{ m}^2 \text{ kg}^{-1}$ |
| u_{sat} | Cubesat length | u_sat | 0.1 m |
| r_g | Displacement of center mass with respect to geometric center | r_g | $[1, 1, 485.3]^T E - 5 \text{ m}$ |
| A_{XZ} | Area of lateral face | A_XZ | 0.06 m ² |
| A_{XY} | Area of top and bottom faces | A_XY | 0.06 m ² |
| A_{panel} | Area of solar panel | A_panel | 0.06 m ² |
| $\rho_{S_{SC}}$ | Specular reflection coefficient of spacecraft surfaces | rho_s_SC | 0.5 |
| $\rho_{D_{SC}}$ | Diffuse reflection coefficient of spacecraft surfaces | rho_d_SC | 0.1 |
| $\rho_{S_{panel}}$ | Specular reflection coefficient of spacecraft solar panel | rho_s_panel | 0.1 |
| $\rho_{D_{panel}}$ | Diffuse reflection coefficient of spacecraft solar panel | rho_d_panel | 0.1 |

Magnetic Field

| Symbol | Description | Code | Value |
|--------|-------------|------|-------|
| | | | |

| | | | |
|-----------------|--|-------------------------|---|
| T_E | Rotation period of Earth around its own axis | <code>T_E</code> | 8.6164×10^4 s |
| ω_E | Angular speed of Earth around its own axis | <code>w_E</code> | 7.2921×10^{-5} rad s ⁻¹ |
| R_E | Earth's Radius | <code>R_E</code> | 6.3712×10^3 km |
| δ_{pole} | Angle between Earth's Magnetic North and Spin Axis | <code>delta_pole</code> | 0.2007 rad |
| m_{SC} | Spacecraft Dipole moment | <code>m_SC</code> | $[0.01, 0.05, 0.01]^T$ A m ⁻² |

Sun related parameters

| Symbol | Description | Code | Value |
|---------------|--------------------------------|----------------------|--|
| T_{Sun} | Period of Earth around Sun | <code>T_sun</code> | 3.1557×10^7 s |
| n_{Sun} | Earth's mean motion around Sun | <code>n_sun</code> | 1.9910 rad s ⁻¹ |
| ε | Ecliptic plane inclination | <code>eclip</code> | 0.4093 rad |
| R_{Sun} | Earth orbit radius around Sun | <code>R_sun</code> | 1.496×10^8 km |
| $F_{e_{Sun}}$ | Solar radiation intensity | <code>Fe_sun</code> | 1358 W m ⁻² |
| P_{Sun} | Solar radiation pressure | <code>P_sun</code> | 4.5298×10^{-6} N m ⁻² |
| c | Speed of light in a vacuum | <code>c_light</code> | $2.997\,924\,58 \times 10^8$ m s ⁻¹ |

Introduction

This report presents the methodology followed for the design and simulation of an Attitude Control System for a Nadir pointing mission in a Low Earth Orbit. The control is tailored to a 12U CubeSat using magnetometers and a horizon sensor for attitude determination and magnetorquers and an inertia wheel for attitude control. The three critical stages of the mission are simulated: detumbling, slew manoeuvre and pointing. A compromise between pointing accuracy, type and number of sensors and actuators and control logic robustness is found and discussed in this document. Spacecraft quaternions and angular velocities are implemented for the physical modelling and control logic. The control is designed with the LQR approach using a proportional controller. The detumbling phase is performed using the *Bdot* method, while the slew and pointing manoeuvre are executed with the proportional controller.

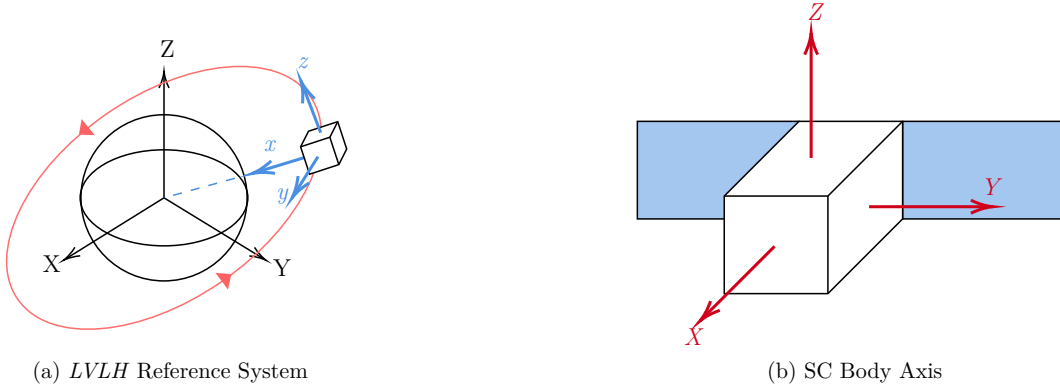
1. Mission Description and Requirements

The assigned mission consists of a 12U CubeSat which shall use a 3 axis magnetometer for Attitude Determination and 3 magnetic rods and an inertia wheel for attitude control. The required specifications for attitude determination include only the 3 axis magnetometer which provides a single measurement vector of the Earth's magnetic field. Given attitude determination methods require the use of at least two linearly independent vectors the decision to add an Earth horizon sensor was made. The sensor was selected because the mission is Earth pointing, meaning no additional slewing than the required for Nadir pointing is needed for its use. The specifications of this sensor are described in 4.2 A LEO orbit is selected given the magnetometer and magnetorquers require the use of a strong magnetic field. The relatively low accuracy of this family of sensors coupled with the low satellite mass requirements of the assigned platform led to the decision of simulating a low-precision Nadir pointing mission. A near circular orbit is selected with the objective of simplifying the control model with a virtually constant angular rate. The specific orbital parameters of the mission are found in Table 1.1.

| Orbital Parameter | Value | Unit |
|--|------------|---------|
| Semi-major axis (a) | 6716.488 | [km] |
| Eccentricity (e) | 0.00771 | [$-$] |
| Inclination (i) | 40.901 | [deg] |
| Right Ascension of the Ascending Node (Ω) | 50.015 | [deg] |
| Argument of Perigee (ω) | 167.166 | [deg] |
| Initial True Anomaly (θ_0) | 0 | [deg] |
| Mean motion (n) | 0.00114698 | [rad/s] |
| Orbital Period (T) | 5478.03 | [s] |

Table 1.1: Orbital Parameters of the Mission

The control follows the *LVLH* reference system as seen in Figure 1.1a. The x Axis of the Body Frame in Figure 1.1b must be aligned to this *LVLH* system to ensure correct pointing. This scheme is explained in Section 5. The onboard camera has a low resolution high shutter speed lens with a large aperture size that allows for less strict drift and pointing error limits. A maximum drift of $10^\circ/\text{s}$ and a pointing error of less than 6° is required by the control system.



1.1 Mission Phases

The mission is divided into three main phases: Detumbling, Slew Manoeuvre and Pointing. The satellite is ejected into its desired orbit by a launcher vehicle with an angular rate of $100^\circ/\text{s}$. The first objective of the control system is to slow this rotation speed down sufficiently to allow for the next phase of the mission; Slew Manoeuvre. In this project, it is considered that the CubeSat is detumbled when the absolute value of its angular rate is less than 0.01 rad/s , which corresponds to almost 1 RPM. This is further explored in Section 5. Attitude Determination can now commence and the satellite initiates its slew manoeuvre to acquire its correct Nadir pointing.

1.2 Spacecraft Geometry

The assigned satellite is a 12U CubeSat. The platform is organized in a $2 \times 2 \times 3$ structure with two adjacent deployable solar panels as seen in Figure 1.2.

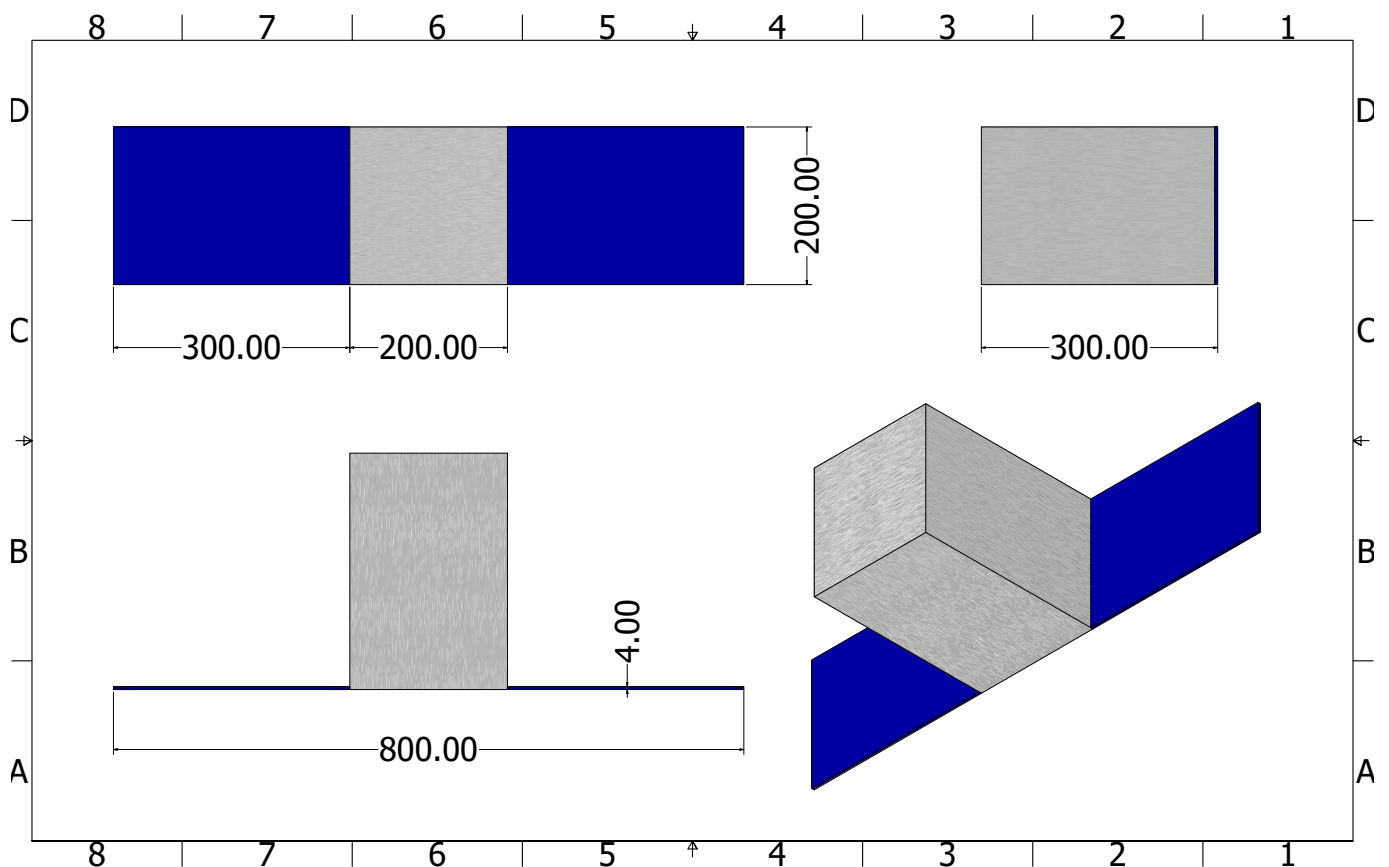


Figure 1.2: Spacecraft Geometry

- $I_x = 0.6324 \text{ kg m}^2$
- $I_y = 0.4084 \text{ kg m}^2$
- $I_z = 0.4491 \text{ kg m}^2$

2. Dynamics and Kinematics modelling

2.1 Dynamics

The dynamics of the system are derived from Euler's Equation for a dual spin spacecraft. The inertia wheel is modelled as spinning at a constant rate. The changes in angular rates are assumed to be instantaneous. The general equation is:

$$\underline{h} = \underline{\underline{J}} * \underline{\omega} + \underline{A} * \underline{h}_r \quad (2.1)$$

Using Euler's Equation

$$\begin{aligned} \dot{\underline{h}} &= \underline{T} \\ \underline{T} &= \underline{\underline{J}} * \dot{\underline{\omega}} + \underline{\omega} \times \underline{\underline{J}} * \underline{\omega} + \underline{\omega} \times \underline{A} * \dot{\underline{h}}_r \end{aligned}$$

Inertia wheel is located in the SC's Z axis, parallel to the angular momentum vector during Nadir pointing, to stabilize the satellite while allowing a better control over the roll axis for pointing manoeuvre. The objective is to store momentum in orbit making it a momentum biased spacecraft. Once the desired attitude is obtained the wheel is sped up making it harder for disturbances to rotate the spacecraft. The inertia wheel is operated at a nominal speed of 1200 RPM, resulting in 0.00612 Nms. This value is varied for active control of the spacecraft and further discussed in Section 6.

Drag torque is secular while magnetic torque and gravity gradient are periodic. When the wheel reaches its maximum speed of 6000 RPM (0.0306 Nms) it is considered to be saturated. De-saturation is performed by returning the wheel to its nominal speed and actuating the magnetorquers. Both environmental and control torques are fed into above equation and solved for the angular rate ω , which is then used in the Kinematics block seen in Section 2.2.

2.2 Kinematics

Due to requirements of this project, quaternions are implemented for Attitude Determination. The ω output of the dynamics block is used to calculate the quaternion time derivative \dot{q} . It is then integrated and normalized to eliminate numerical errors. This output is subsequently converted into the A_{BN} rotation matrix from inertial to body axis. This conversion is done to ease the troubleshooting process and better visual understanding of the behaviour of the spacecraft.

$$\frac{dq}{dt} = \frac{1}{2} \begin{bmatrix} 0 & \omega_w & -\omega_v & \omega_u \\ -\omega_w & 0 & -\omega_u & \omega_v \\ \omega_v & -\omega_u & 0 & \omega_w \\ -\omega_u & -\omega_v & -\omega_w & 0 \end{bmatrix} q(t) \quad (2.2)$$

3. Environment modelling

3.1 Environment modelling

The simulation propagates the orbit and models the principal disturbing torques acting on the spacecraft. The order of magnitude of all disturbances was estimated for an altitude of 350km, assuming a C_{Drag} of 2.2 and using geometric characteristics from the Star of Aoxiang mission[1]. The results are presented in Table 3.1 with the two largest disturbances being the aerodynamic drag and the magnetic disturbance torque. Initially gravity gradient and solar radiation pressure were discarded and not modelled. Gravity gradient was added in order to increase the rank of the state space representation. The table also presents the maximum torques from the simulation output. Simulation values are comparable to the preliminaries, validating the calculations.

| Disturbance | Preliminary max value [Nm] | Simulation max value [Nm] |
|--------------------------|----------------------------|---------------------------|
| Aerodynamic Drag | 2.89e-5 | 1.76e-5 |
| Magnetic Disturbance | 2.55e-6 | 2.71e-6 |
| Gravity Gradient | 4.40e-7 | 4.52e-7 |
| Solar Radiation Pressure | 1.14e-7 | - |

Table 3.1: Disturbance torques

3.1.1 Orbit Propagation

The orbit is propagated at every time step of the simulation. The true anomaly is integrated using equation 3.1 the orbital position vector is then calculated using equation 3.2. The position vector is finally converted to the inertial frame.

$$\dot{\theta} = \frac{n(1 + e \cos \theta)}{(1 - e^2)^{3/2}} \quad (3.1)$$

$$R = \frac{a(1 - e^2)}{1 + e \cos \theta} \quad (3.2)$$

3.1.2 Aerodynamic Drag

Aerodynamic Drag is modelled using the procedure outlined in [2]. The density model is an exponential model with values listed in 3.2. The atmosphere is assumed to depend only on altitude and constant in time. Only values accounting for the minimum (286 km) and maximum altitudes (390 km) are listed. The density at a point is calculated using 3.3

$$\rho = \rho_{ref} * e^{\frac{-(h-h_{ref})}{H_0}} \quad (3.3)$$

| Ref. altitude h [km] | Ref. Density ρ [kg/m ³] | Scale Height H_0 [km] |
|------------------------|--|-------------------------|
| 250 | 7.248e-11 | 45.546 |
| 300 | 2.418e-11 | 53.628 |
| 350 | 9.158e-12 | 53.298 |

Table 3.2: Density Model

The drag is verified by comparing it to the NRLMSISE-00, a high fidelity experimental model that considers geodetic coordinates, magnetic index and solar flux variations. The comparison is done for an equatorial orbit with an initial attitude where the solar panels are radially aligned to the Earth, such that drag is maximum. Figure 3.1 shows the correlation between the model and the NRLMSISE-00 over an orbital period. The same order of magnitude and trend is achieved with a much simpler model. The Z-axis (direction of angular momentum) has a torque one order of magnitude higher than the other two. This is expected for our initial attitude. The positive value in the Z-axis also correctly models the expected initial rotation. A visualization of this behaviour is included in the MATLAB files.

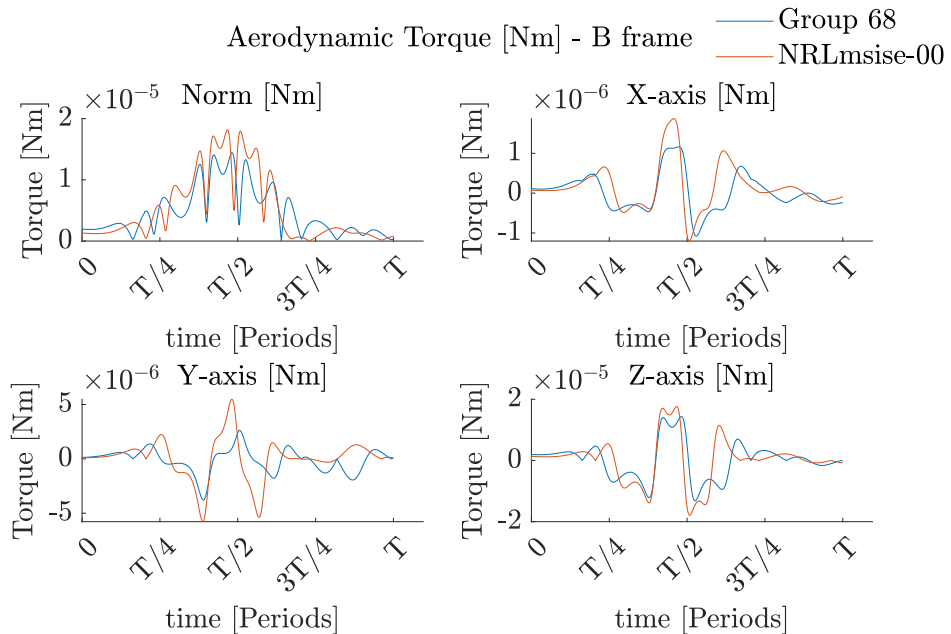


Figure 3.1: Air Drag Validation

Validation

3.1.3 Magnetic Field and Disturbance

The spacecraft's magnetic dipole was obtained from [2] and represents a conservative scenario for estimating torque

$$m_{SC} = [0.01; 0.05; 0.01][A * m^2] \quad (3.4)$$

The magnetic field is modelled from the International Geomagnetic Reference Field (IGRF) 2020 13th order model and is validated by comparing it to Matlab's *igrfmagm* function over three periods. The comparison between the fields can be seen in Figure 3.2. The models almost completely overlap.

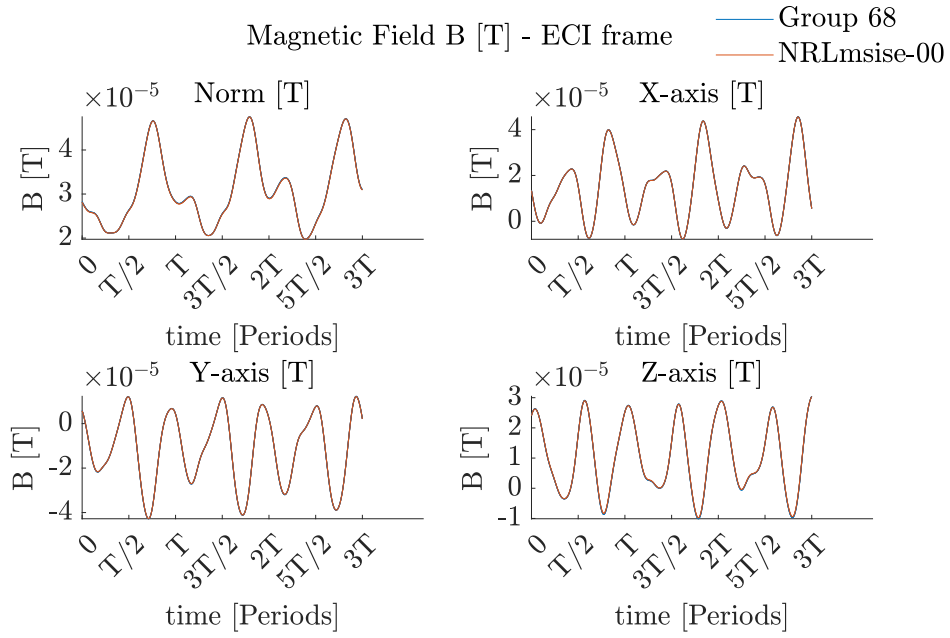


Figure 3.2: Magnetic Field Validation

3.1.4 Gravity Gradient

The gravity gradient is modelled using the equations from [2]. Figure 3.3 shows the gravity gradient in the LVLH frame over five periods. This matches the expected behaviour of the torque mainly acting on the roll and pitch axis and being minimal in the yaw axis.

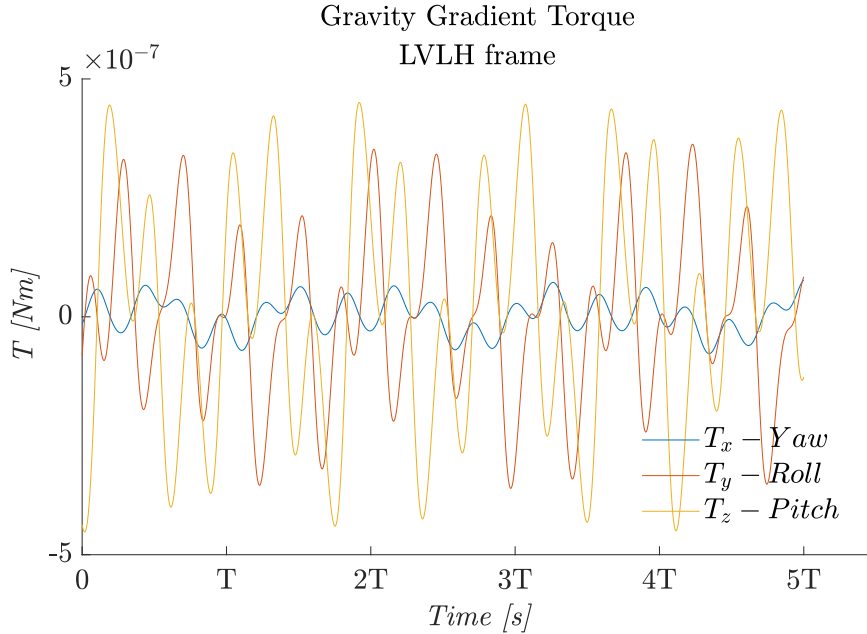


Figure 3.3: Gravity Gradient Validation

4. Sensor modelling

4.1 Sensors

4.1.1 Magnetometer - HMC5983

The Honeywell HMC5983 is a temperature compensated three-axis integrated circuit e-compass specifically designed for low-field magnetic sensing, exactly as the mission performed by the satellite on this report. The sensor's specifications are [3]:

- Dimensions: 3x3x0.9 mm.
- Digital resolution: $7.3 \cdot 10^{-8}$ T - $4.35 \cdot 10^{-7}$ T.
- Noise floor: $2 \cdot 10^{-7}$ T.
- Output rate: 0.75 Hz - 220 Hz.

4.1.2 Earth Horizon Sensor - CubeSense Earth Gen 2

The Cubespace CubeSense Earth Gen 2 is an infrared horizon sensor capable of providing high accuracy roll and pitch determination. The sensor's specifications are [4]:

- Dimensions: 35x24x20 mm.
- Accuracy: 1 deg (roll and elevation).
- Update rate: Up to 2 Hz.



Figure 4.1: Magnetometer - HMC5983



Figure 4.2: Earth Horizon - CubeSense

4.2 Sensor modelling

The sensors described above are used to provide the attitude determination of the spacecraft through their appropriate modelling in the simulation. Two different types of sensor are being used as it is necessary to have at least two independent measurements.

4.2.1 Magnetometer

The magnetometer must be coupled with a mathematical model of the magnetic field which depends on the position of the satellite (provided by the environment) and supplies the magnetic field in inertial reference frame. In our model, measuring the magnetic field means converting the magnetic field from inertial to body frame using the DCM representing the spacecraft attitude through the equation 4.1 and then adding noise on it.

$$b_B = A_{B/N} b_N \quad (4.1)$$

To model it inside the simulation the following procedure is followed:

- The non-orthogonality of the axes system is considered creating a rotation matrix A_ϵ where α , β and γ are really small angles obtained through the literature [5].

$$A_\epsilon = \begin{bmatrix} 1 & 0 & \alpha \\ \beta & 1 & \gamma \\ 0 & 0 & 1 \end{bmatrix}$$

- The mounting error of the sensor is obtained using a rotation matrix 313, R_{313} , where a1, a2 and a3 are random small rotation angles around x, y and z axis respectively.

$$R_{313} = \begin{bmatrix} 1 & a1 + a3 & 0 \\ -a1 - a3 & 1 & a2 \\ 0 & -a2 & 1 \end{bmatrix}$$

- The matrix R_{313} is premultiplied by A_ϵ in order to combine both errors. The resultant matrix multiplies the A_{BN} that comes from kinematics.
- The magnetic field in inertial frame estimated in the environment block is premultiplied by the matrix obtained in the previous point and the measured magnetic field in body frame is obtained. Then, the result is rounded according to the digital resolution of the magnetometer.
- To introduce the measured body frame magnetic field vector in a more realistic way, a Gaussian noise with zero mean and amplitude of the sensor's noise floor is introduced.
- Finally, the signal is discretized looking at the output rate of the sensor and choosing the more appropriate value for the simulation.

4.2.2 Earth Horizon Sensor

An infrared horizon sensor measures the infrared radiation from Space and from Earth in order to obtain the precise position of the centre of the planet. A horizon sensor's work principle is based on using thermopile detectors to compute the direction vector of the Earth with respect to the spacecraft. To model it, almost the same procedure as for the magnetometer is followed. The difference is that instead of using the magnetic field estimated in the environment block, the sensor is inputted with the position of the spacecraft with respect the Earth in inertial frame. There is no rounding based on the resolution as no information is provided in the datasheet.

4.3 Attitude Determination - Algebraic Method

The algebraic method [6] is applied with the two independent measurements to calculate the spacecraft's attitude. The procedure is the following:

- The two independent normalized measurements p and q and their corresponding directions in the inertial reference system a and b are used.
- The following component vectors are created:

$$\begin{aligned} s_1 &= p & v_1 &= a \\ s_2 &= \frac{p \wedge q}{|p \wedge q|} & v_2 &= \frac{a \wedge b}{|a \wedge b|} \\ s_3 &= p \wedge s_2 & v_3 &= a \wedge v_2 \end{aligned}$$

- The three unit vectors s_1, s_2, s_3 are orthogonal to each other and are used to create the matrix S. Similarly v_1, v_2, v_3 are used to create the matrix V. The DCM of the spacecraft's body frame with respect to the inertial frame can then be obtained through Equation 4.2

$$A_{B/N} = SV^{-1} = SV^T \quad (4.2)$$

5. Control Logic

The control logic is split in two main control algorithms pertaining to the mission phases:

- Detumbling: B-Dot logic which only requires magnetometers and magnetorquers.
- Slew manoeuvre and nadir pointing: Linear Quadratic Regulator (LQR) logic and Linear Quadratic Estimator (LQE) observer which uses all the sensors and actuators on board.

Instead of using two separate Simulink files in each phase, the control logic is divided in two using *enabled subsystems* that are chosen based on an *if-condition* and a counter. Both control algorithms work using the same principle and have a similar state-space representation. The system works with the following procedure:

- The counter begins at zero and increases by one when each component of the angular velocity is considered detumbled ($\omega - 0.01 \text{ [rad/s]}$ and 0.01 [rad/s]) . The counter is reset to zero if one component drifts outside of these boundaries.
- While the output of the counter is less than 100 the detumbling logic is used.
- While the output of the counter is more than 100 the slew and pointing logic is used.

5.1 Detumbling - B-Dot Method

The B-Dot logic is a nonlinear attitude control technique based on magnetometers as sensors and magnetorquers as actuators. It is a powerful tool for LEO satellites which makes use of the strong magnetic field in low altitudes. Despite the fact that it does not offer a precise control, it is the simplest to implement, having great advantages in terms of difficulty and cost [7]. The control to be generated by the actuators is obtained using Equation 5.1, where \underline{M}_c is the control torque, \underline{m} is the magnetic dipole generated by the actuators and \underline{B} is the magnetic field.

$$\underline{M}_c = \underline{m} \wedge \underline{B} \quad (5.1)$$

The main difficulty consists on obtaining the magnetic dipole that needs to be generated. In this project, the B-Dot Bang Bang method is implemented which uses the maximum dipole that can be generated by the actuators, m_{max} , whose sign is based on the sign of the variation of the magnetic field, $\dot{\underline{B}}_m$.

$$\underline{m} = -m_{max} \text{sign}(\dot{\underline{B}}_m) \quad (5.2)$$

5.2 Slew Manoeuvre and Nadir Pointing - LQR and LQE logic

The optimal control is a linear attitude control based on state-space representation [7]. In this case, the LQR is used for the control while the LQE is used for the observer. This allows for a full estimation of the state to be obtained even though it cannot be entirely measured.

The control logic is divided again differentiating between the slew and the nadir pointing. The split is performed using an *if-condition*. The main difference is that for the slew manoeuvre the inertia wheel is powered up while for the nadir pointing it maintains with a nominal speed. This is a logical decision as the dual-spin stabilization is used to stabilize the spacecraft along one axis. If the CubeSat is not in the proper orientation, applying nominal speed to the axis will make slewing to the correct position harder and it will be considered a source of perturbations for the control. The *if-condition* is similar to the one used to select between detumbling and slew and nadir pointing.

- The counter adds one unit when the norm of the quaternions error is between -0.05 and 0.05 and every time that the norm is outside these boundaries the counter is reset to 0.
- While the output of the counter is less than 1000 the slew logic is used.
- While the output of the counter is more than 1000 the control logic is changed to nadir pointing.

5.2.1 State-Space Representation

The Space State representation

$$\begin{cases} \dot{\underline{x}} = \underline{\underline{A}} \underline{x} + \underline{\underline{B}} \underline{u} \\ \underline{y} = \underline{\underline{C}} \underline{x} + \underline{\underline{D}} \underline{u} \end{cases} \quad (5.3)$$

with

$$\underline{x} = [q_1, q_2, q_3, \omega_x, \omega_y, \omega_z]$$

is written following a linearization of the spacecraft dynamic and quaternions' kinematics ($\dot{q} = \frac{1}{2}\Omega q$) around equilibrium condition to fulfill nadir pointing:

$$\underline{x}|_{q \approx [0,0,0,1], \underline{\omega} \approx [0,0,0]} = [0, 0, 0, 0, 0, 0] \quad (5.4)$$

In this case the quaternions (scalar last) are expressing the rotation between LVLH and ECI in body frame and \underline{u} is the angular velocity between body frame and LVLH expressed in body frame. The gravity gradient torque must be added in the dynamics equation to get the maximum rank of the controllability matrix.

After linearization the following matrices are obtained:

$$A = \begin{bmatrix} 0 & 0 & 0 & \frac{1}{2} & 0 & 0 \\ 0 & 0 & 0 & 0 & \frac{1}{2} & 0 \\ 0 & 0 & 0 & 0 & 0 & \frac{1}{2} \\ \frac{-2n(n(I_z - I_y) - H_r)}{I_x} & 0 & 0 & 0 & (I_x + I_y - I_z)n - H_r & 0 \\ 0 & \frac{2n(4n(I_x - I_z) - H_r)}{I_y} & 0 & -(I_x + I_y + I_z)n + H_r & 0 & 0 \\ 0 & 0 & -6n^2(I_y - I_x) & 0 & 0 & 0 \end{bmatrix},$$

$$B = \begin{bmatrix} 0 & 0 & 0 \\ 0 & 0 & 0 \\ 0 & 0 & 0 \\ \frac{1}{I_x} & 0 & 0 \\ 0 & \frac{1}{I_y} & 0 \\ 0 & 0 & \frac{1}{I_z} \end{bmatrix}, C = \begin{bmatrix} 1 & 0 & 0 & 0 & 0 & 0 \\ 0 & 1 & 0 & 0 & 0 & 0 \\ 0 & 0 & 1 & 0 & 0 & 0 \end{bmatrix}, D = \begin{bmatrix} 0 & 0 & 0 \\ 0 & 0 & 0 \\ 0 & 0 & 0 \end{bmatrix}$$

where n is the angular velocity related to one orbital period. In the case of the slew manoeuvre the state-space representation is almost identical, but H_r is set to zero as the nominal speed of the wheel is zero. Ranks of the controllability and observability matrices are checked using Matlab functions [8].

5.2.2 Control Design

To use LQR for control and LQE for the observer it is necessary to select values for the Q and R matrices. Using suggestions for these from literature made our dynamic model work only for the linear state space model but not for the real one. After deeply understanding the meaning of the single terms several simulations were conducted iterating on what should get more importance between the control and state information. The following Q and R matrices are the outcome of the previous campaign.

$$Q_{lqr} = \begin{bmatrix} 1e-3 & 0 & 0 & 0 & 0 & 0 \\ 0 & 1e-3 & 0 & 0 & 0 & 0 \\ 0 & 0 & 1e-3 & 0 & 0 & 0 \\ 0 & 0 & 0 & 0.1 & 0 & 0 \\ 0 & 0 & 0 & 0 & 0.1 & 0 \\ 0 & 0 & 0 & 0 & 0 & 0.1 \end{bmatrix}, R_{lqr} = \begin{bmatrix} 100 & 0 & 0 \\ 0 & 100 & 0 \\ 0 & 0 & 100 \end{bmatrix};$$

$$Q_{lqe} = \begin{bmatrix} 0.05 & 0 & 0 \\ 0 & 0.05 & 0 \\ 0 & 0 & 0.05 \end{bmatrix}, R_{lqe} = \begin{bmatrix} 100 & 0 & 0 \\ 0 & 100 & 0 \\ 0 & 0 & 100 \end{bmatrix}$$

After the Q and R matrices are defined the next step is to derive the gain matrix K. The solution to Riccati's Equation (S) which governs optimal control is used to obtain K. The functions implemented in Matlab for this purpose are used:

$$[K, S, E] = lqr(A, B, Q_{lqr}, R_{lqr})$$

where E is a vector containing the poles of the close loop system. In the Simulink model, the control torque is obtained by multiplying K with the observed state ($Mc = -K\hat{x}$). Modelling of the observer has a very similar procedure: L is obtained by the Matlab function

$$[L, P, E] = lqe(A, B, Q_{lqe}, R_{lqe})$$

In this project the real measurement \underline{y} is considered to be the quaternion representing the rotation between LVLH and body frame which is derived from the measured $A_{B/N}$ by multiplying it to $A_{L/N}$, that depends only on the true anomaly of spacecraft known from the environment, to obtain $A_{B/L}$ which can be converted to the corresponding quaternion.

6. Actuator modelling

6.1 Actuator Modelling

The assigned actuators are 3 magnetorquers and 1 inertial wheel. The selection is done using an estimation of the required control torque in the different phases of the mission by considering the maximum disturbance torques listed in table 3.1 and taking into account a size limit imposed by the dimensions of the CubeSat.



Figure 6.1: Magnetorquer - CR0020

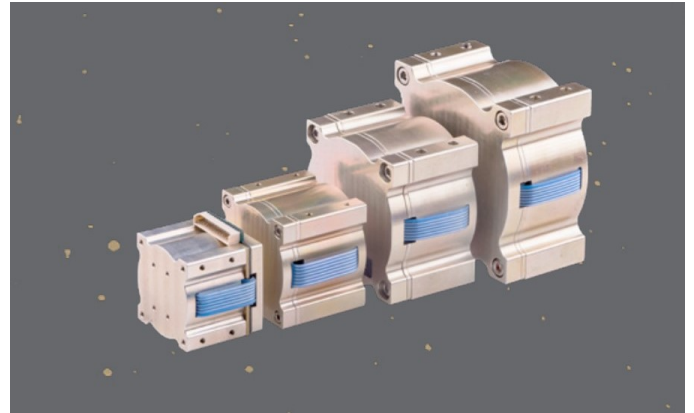


Figure 6.2: Inertial Wheel - CubeWheel L

Magnetorquer:

- x-axis (ZarmTechnik MT5-2)
 - Dimensions: 18x18x240 mm.
 - Mass: 300 g
 - Magnetic Moment: $\pm 5.0 \text{ Am}^2$
- y-axis/z-axis (CubeSpace CR0020)
 - Dimensions: 13x13x152 mm.
 - Mass: 54 g
 - Magnetic Moment: $\pm 2.0 \text{ Am}^2$

Inertial Wheel:

- z-axis (CubeSpace CubeWheel L)
 - Dimensions: 57x57x31.5 mm.
 - Mass: 225 g
 - Speed Range: $\pm 6000 \text{ RPM}$
 - Max Momentum: 30.6 mNm
 - Max Torque: 2.3mNm

To choose the three magnetorquers, the value considered is the maximum magnetic moment and the available maximum length along each axis. One magnetorquer is installed along each body frame axis. For the wheel considerations are made on maximum momentum and maximum torque. The inertial wheel is installed with the spinning axis parallel to the angular momentum vector of the orbit during nadir pointing as explained in 2.2. The inertial wheel has a nominal speed of 1200 RPM, 1/5 of the maximum to prevent immediate saturation but still provide enough momentum to stabilize the spacecraft.

6.1.1 Detumbling

In detumbling mode the actuators are modelled as a simple cross product between the maximum magnetic moment available and the measured magnetic field without any further internal electrical modelling. With the previous choice of maximum magnetic moment it takes almost 5 orbits to bring the angular velocity from an initial value of $100^\circ/\text{s}$ to $0.5^\circ/\text{s}$

6.1.2 Slew and Pointing

In this phase of the mission both inertial wheel and magnetorquers are used together. Once the required control torque is calculated in the control block it is necessary to compute the wheel's contribution \dot{H}_r , and the magnetic moments D_x and D_y . This is performed by taking the inverse of:

$$\begin{pmatrix} M_x \\ M_y \\ M_z \end{pmatrix} = \begin{pmatrix} B_x \\ B_y \\ B_z \end{pmatrix} \wedge \begin{pmatrix} D_x \\ D_y \\ 0 \end{pmatrix} - \begin{pmatrix} w_x \\ w_y \\ w_z \end{pmatrix} \wedge \begin{pmatrix} 0 \\ 0 \\ H_r \end{pmatrix} - \begin{pmatrix} 0 \\ 0 \\ \dot{H}_r \end{pmatrix} \quad (6.1)$$

The term $w \wedge h_r$ is considered as part of the dynamics and included in the dynamics block, not in the actuators block. This is done to achieve maximum rank of controllability matrix in the linearized model. It can be computed after the integration of \dot{H}_r obtained from the inverse of

$$\underline{Mc} = \underline{B} \wedge [D_x, D_y, 0]' - \dot{\underline{h}}_r \quad (6.2)$$

As following

$$\begin{pmatrix} D_x \\ D_y \\ \dot{H}_r \end{pmatrix} = \frac{1}{B_z} \begin{bmatrix} 0 & -1 & 0 \\ 1 & 0 & 0 \\ -B_x & -B_y & -B_z \end{bmatrix} \begin{pmatrix} M_x \\ M_y \\ M_z \end{pmatrix}. \quad (6.3)$$

During the slew manoeuvre the integration of \dot{H}_r starts from a null initial condition while during the pointing manoeuvre the integration of \dot{H}_r starts from the last value of the slew. In order to avoid overshoot and stabilize the control a maximum value of $H_r = H_{rmax}/6$ is chosen during the slew manoeuvre and the maximum torque is limited to $\dot{H}_r = \dot{H}_{rmax}/10$ in both slew and pointing. The magnetorquers don't destabilize the spacecraft because of overshoot or a too high control torque so their actual maximum magnetic momentum is not limited.

$[D_x, D_y, \dot{H}_r]$ are used to compute the actual torque that will be provided by the actuators. For the magnetorquers:

$$\underline{T_c} = \underline{B} \wedge [D_x, D_y, 0]' \quad (6.4)$$

while for the inertial wheel \dot{H}_r is the torque along z axis though still it needs to be integrated as mentioned previously. The two control torque contribution are then added and sent to the dynamics block where the whole loop is finally closed.

7. Simulation

The outline of the Simulink model can be seen in 7.1. The simulation is performed over a period of 10 orbits. The initial rotation rates are 100 degrees per second for each axis, representing a case where the spacecraft is spinning much faster than the instrument requires to operate and is unable to complete the mission objective. The comparison of the spacecraft's behaviour and performance for both the uncontrolled and controlled case is done in the following paragraphs.

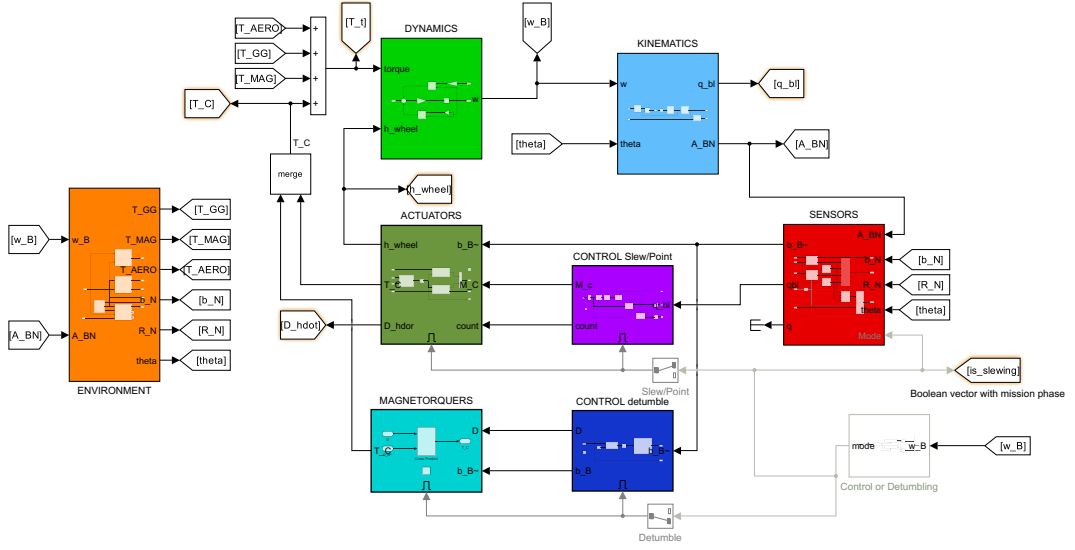


Figure 7.1: Simulink Model

7.1 Angular Rates

Figure 7.2a shows the behaviour of the angular rates when no control is in place. The time evolution of the rotation is chaotic and altered only by the disturbance torques. The slew and Nadir pointing control logic is never activated. Figure 7.2b shows the behaviour when the control is enabled. The initial tumbling rates converge in three periods allowing for the slew and pointing control logic to activate. The slew manoeuvre and the pointing barely alter the rotation rates which remain in the not-tumbling limits for the remaining orbits. The improvement from the control implementation is clear.

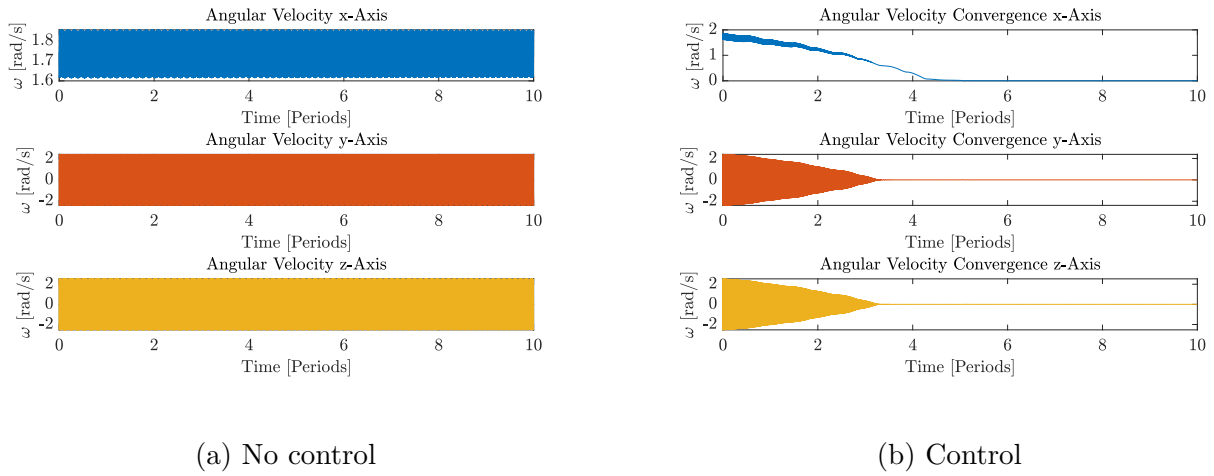


Figure 7.2: Time evolution of angular velocities

7.2 Pointing performance

The performance is measured by the pointing error as shown in the figures below. 7.4 shows the performance when no control is in place. In 7.4a the pointing is almost never below the objective, as shown by the red line representing the maximum permissible pointing error. The red area in the lower left corner of 7.4b is the region where the drift is in the acceptable region. The mission performance of the no control case is dreadful. Figures 7.4c and 7.4d shows the pointing performance when the control is enabled, with the x axis representing time since the pointing control has been activated. The pointing error is consistently below the boundary and averages 1.3 degrees of error as shown in 7.4c. The drift versus FOV performance is always in the region as shown in 7.4d. The performance of the system when the control is activated satisfies the mission requirements with ease.

The pointing error of the controlled action can be fitted to a Weibull distribution as seen in Figure 7.3. This distribution serves to prove the reliability of the control system. The skewed left scattering shows a low average pointing error, with most values concentrated in a low error region.

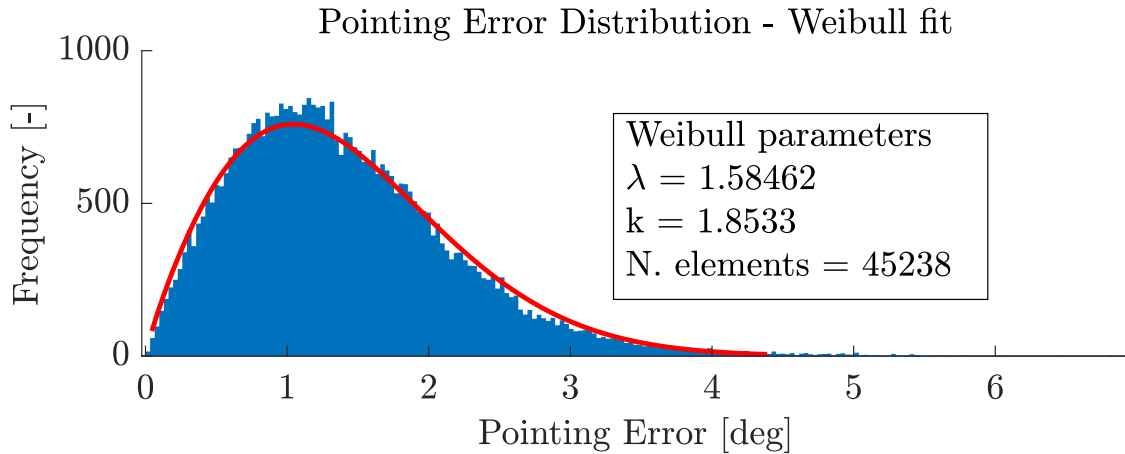


Figure 7.3: Pointing Error Distribution

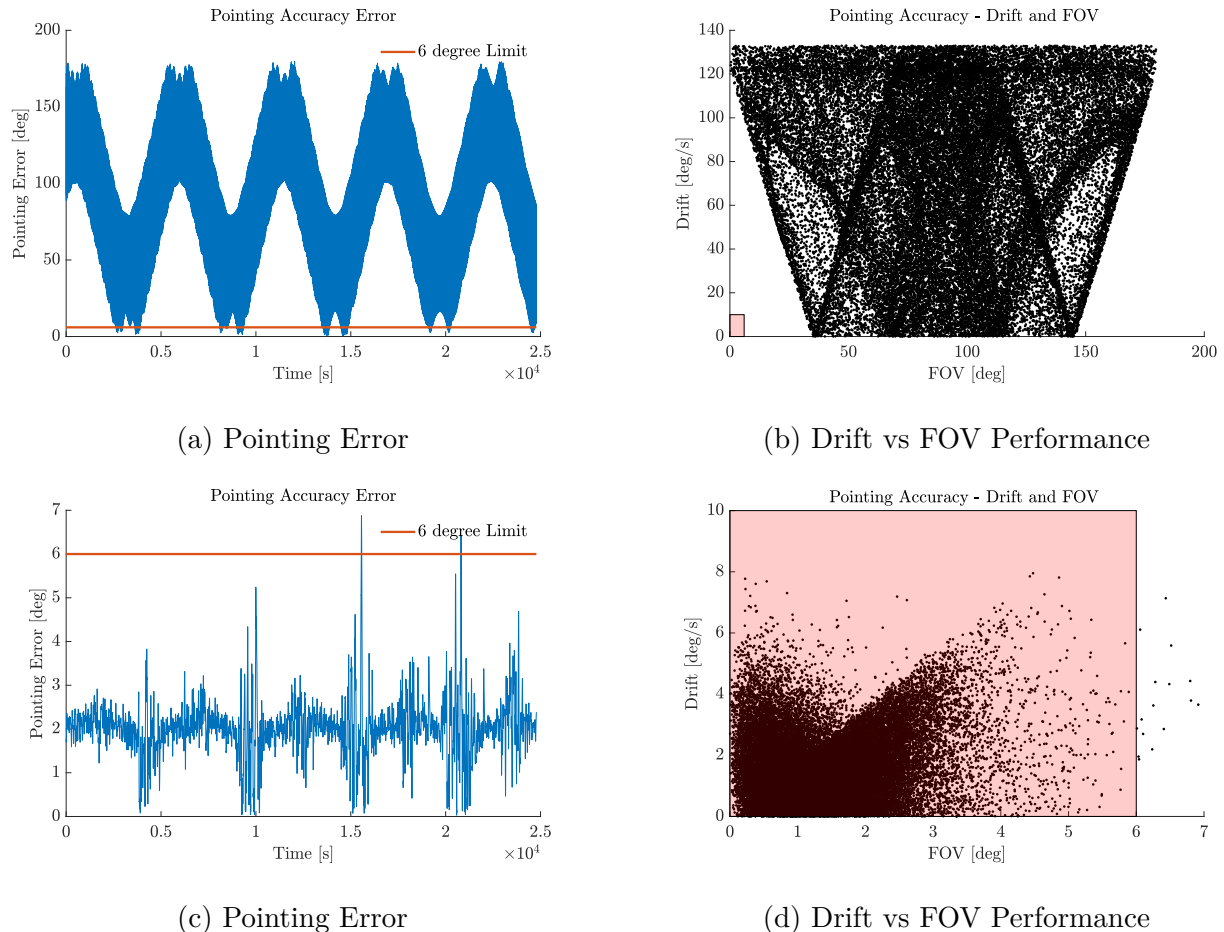


Figure 7.4: SC pointing performance - No Control vs Control

Furthermore, 7.5 showcases the evolution of the error in the quaternions of the spacecraft. The scalar part of the quaternion converge to the desired value of 1, indicating proper pointing, whilst the vector component error rapidly decay to zero once the slew manoeuvre commences.

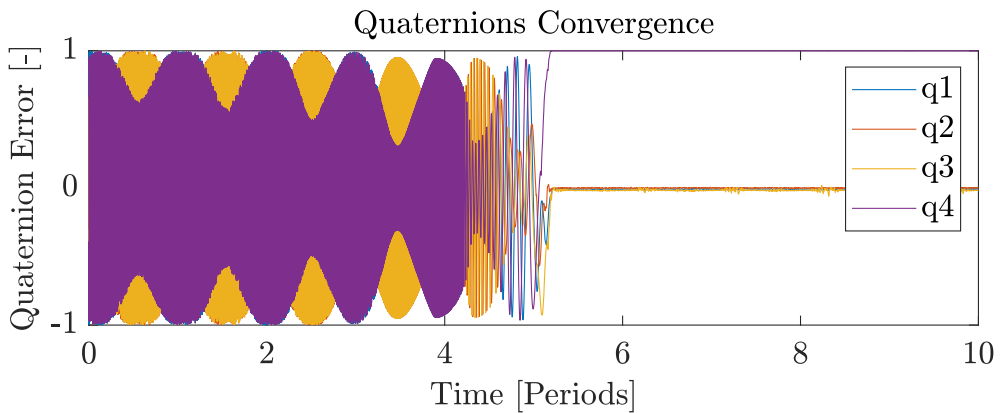


Figure 7.5: Time Evolution of quaternions - Control enabled

Conclusion

This report outlines the design process and rationale for an Attitude Determination and Control system applicable to a Nadir pointing 12U Cubesat in LEO orbit. System dynamics, kinematics, and environmental disturbances are successfully modelled and validated in Simulink. Attitude determination is performed using the algebraic method with measurements from a 3-axis magnetometer and an Earth horizon sensor. The switch between detumbling and slew and pointing mode are implemented. Detumbling is performed using the B_{dot} Bang-Bang technique for three magnetic rods. Slewing and pointing control is done by a LQR and LQE observer using three magnetic rods and an inertia wheel. Beginning from high angular tumbling rates, the system successfully detumbles the satellite, slews and maintains Nadir pointing orientation in less than ten orbital periods. The benefits of the implemented control are clearly highlighted and the comparison to the uncontrolled system is performed.

Bibliography

- [1] Xiaozhou Yu et al. "Star of AOXiang: An innovative 12U CubeSat to demonstrate polarized light navigation and microgravity measurement". In: *Acta Astronautica* 147 (2018), pp. 97–106. ISSN: 0094-5765. DOI: <https://doi.org/10.1016/j.actaastro.2018.03.014>. URL: <https://www.sciencedirect.com/science/article/pii/S0094576517302849>.
- [2] Franco Bernelli Zazzera. *Course Notes - Spacecraft Attitude Dynamics and Control - Part 1: Attitude dynamics and kinematics*.
- [3] Honeywell. *3-Axis Digital Compass IC HMC5983*. URL: https://www.farnell.com/datasheets/1509871.pdf?_ga=2.219060057.1318745487.1555987311-293789508.1555987311.
- [4] Cubespace. *CubeSense Earth Gen 2*. URL: <https://www.cubespace.co.za/products/gen-2/sensors/cubesense-earth/>.
- [5] Dafeng Long et al. "A Fast Calibration and Compensation Method for Magnetometers in Strap-Down Spinning Projectiles". In: *Sensors* 18.12 (2018). ISSN: 1424-8220. DOI: 10.3390/s18124157. URL: <https://www.mdpi.com/1424-8220/18/12/4157>.
- [6] Franco Bernelli Zazzera. *Course Notes - Spacecraft Attitude Dynamics and Control - Part 2: Attitude sensors and actuators, attitude determination*.
- [7] Franco Bernelli Zazzera. *Course Notes - Spacecraft Attitude Dynamics and Control - Part 3: Introduction to state-space control and attitude control*.
- [8] Y. Yang. "Spacecraft attitude determination and control: Quaternion based method". In: *Annual Reviews in Control* 36.2 (2012), pp. 198–219. ISSN: 1367-5788. DOI: <https://doi.org/10.1016/j.arcontrol.2012.09.003>. URL: <https://www.sciencedirect.com/science/article/pii/S1367578812000387>.